Journal of Physics and Chemistry of Solids 86 (2015) 131–137

Contents lists available at ScienceDirect

Journal of Physics and Chemistry of Solids

journal homepage: www.elsevier.com/locate/jpcs

# Phase transformation of strontium hexagonal ferrite

V. Bilovol [a,b,d], R. Martínez-García [c,d,*]

[a] Instituto de Tecnología en Polímeros y Nanotecnología, Facultad de Ingeniería, CONICET - Universidad de Buenos Aires, Av. Gral. Las Heras 2214, CP1127 Buenos Aires, Argentina
[b] Laboratorio de Sólidos Amorfos, INTECIN, Facultad de Ingeniería, Universidad de Buenos Aires, Paseo Colón 850, C1063ACV Buenos Aires, Argentina
[c] Facultad de Recursos Naturales, Universidad Nacional de Formosa – CONICET, Campus Universitario, Modulo I, Av. Gutnisky 3200, Formosa, Argentina
[d] Consejo Nacional de Investigaciones Científicas y Técnicas (CONICET), Argentina

ARTICLE INFO

*Article history:*
Received 3 October 2014
Received in revised form
19 June 2015
Accepted 6 July 2015
Available online 7 July 2015

*Keywords:*
Oxides
Phase transition
MÖssbauer spectroscopy
X-ray diffraction

ABSTRACT

The phase transformation of strontium hexagonal ferrite ($SrFe_{12}O_{19}$) to magnetite ($Fe_3O_4$) as main phase and strontium carbonate ($SrCO_3$) as secondary phase is reported here. $SrFe_{12}O_{19}$ powder was obtained by a heat treatment at 250 °C under controlled oxygen flow. It was observed that the phase transformation occurred when the $SrFe_{12}O_{19}$ ferrite was heated up to 625 °C in confinement conditions. This transformation took place by a combination of three factors: the presence of stresses in the crystal lattice of $SrFe_{12}O_{19}$ due to a low synthesis temperature, the reduction of $Fe^{3+}$ to $Fe^{2+}$ during the heating up to 625 °C, and the similarity of the coordination spheres of the iron atoms present in the S-block of $SrFe_{12}O_{19}$ and $Fe_3O_4$. X-ray diffraction analysis confirmed the existence of strain and crystal deformation in $SrFe_{12}O_{19}$ and the absence of them in the material after the phase transformation. Dispersive X-ray absorption spectroscopy and $Fe^{57}$ Mössbauer spectroscopy provided evidences of the reduction of $Fe^{3+}$ to $Fe^{2+}$ in the $SrFe_{12}O_{19}$ crystal.



## 1. Introduction

The strontium hexagonal ferrite ($SrFe_{12}O_{19}$) has been extensively studied from the middle of XX century [1,2]. Due to its magnetic properties (uniaxial anisotropy and high magnetization) it has been used as a permanent magnet and as information storage media [3–7]. The ceramic method, the first method used to obtain $SrFe_{12}O_{19}$, requires heating up to 1200 °C [8]. In order to decrease the synthesis temperature, chemical methods, like sol–gel and co-precipitation have been developed. Such methods involve heat treatments between 800 °C and 1000 °C [9–18]. Moreover, some variations of these methods allow synthesizing hexagonal ferrites at temperatures below 500 °C [13,17,19].

$SrFe_{12}O_{19}$ synthesized at low temperatures has been extensively characterized structurally and magnetically, but there are few studies about the thermal stability of the obtained material [20]. Due to low temperature involved in the synthesis, the hexagonal ferrite could have crystal imperfections and some structural stresses. In our previous work we reported experimental evidence about the metastability of $SrFe_{12}O_{19}$ powder obtained at 400 °C under oxygen flow [21]. To our knowledge, there are no other reports on the subject.

The aim of this paper is to report the phase transformation of $SrFe_{12}O_{19}$ to magnetite ($Fe_3O_4$) and strontium carbonate ($SrCO_3$). The factors that promote this phase transformation were analyzed. Interestingly and by the first time to our knowledge, the $Fe^{3+}$ to $Fe^{2+}$ reduction in the $SrFe_{12}O_{19}$ crystal is reported here.

## 2. Materials and methods

The $SrFe_{12}O_{19}$ powder was obtained using the sol–gel method with organometallic hexaferrite as precursor [14,22]. For this purpose, a highly concentrated ferric nitrate solution with citric acid as the primary coordinator agent was prepared. In order to achieve the atomic ratio Fe/Sr = 12, a proper amount of $SrCO_3$ was added. After that, benzoic acid and ethylene glycol (secondary coordinators agents) were added. Then, the clear solution was slowly evaporated. During the process, $NO_3$ group was decomposed emitting nitrous gases ($NO^-$ and $NO_2$). The thermal treatment produced the emission of $CO^-$, $CO_2$ and $H_2O$ as well. The heating was maintained until the gel was dried forming a viscous residue. To obtain $SrFe_{12}O_{19}$, the dried gel (organometallic hexaferrite) was thermally treated for 3 h at 250 °C under an oxygen flow of 200 $cm^3$/min.

In order to induce the phase transformation of the $SrFe_{12}O_{19}$ a heat treatment was performed. The treatment was carried out

* Corresponding author at: Facultad de Recursos Naturales, Universidad Nacional de Formosa – CONICET, Campus Universitario, Modulo I, Av. Gutnisky 3200, Formosa, Argentina.
*E-mail address:* rmartinez@fi.uba.ar (R. Martínez-García).

http://dx.doi.org/10.1016/j.jpcs.2015.07.006
0022-3697/

from room temperature to 625 °C at a rate of 5 °C/min with the sample placed in a closed capsule of aluminum.

The study of the phase transformation was carried out with a combination of spectroscopic techniques. It is well known that X-ray absorption near edge structure technique is very sensitive to changes in oxidation state of the material under research. On the other hand, $^{57}$Fe Mössbauer spectroscopy (MS) was employed to corroborate the degree of oxidation state of iron. Both techniques combined with X-ray diffraction (XRD) allow performing the accurate identification of iron oxide involved in the phase transformation. Furthermore, MS and magnetometry techniques contribute to the characterization of the magnetic phases involved in the process.

Structural properties of the powders used in this report were analyzed by XRD in a $\theta$–$2\theta$ diffractometer (Rigaku D/max equipped with a vertical goniometer) using Cu–$K_\alpha$ radiation. The average crystallite size of the phases involved was calculated using the Scherrer equation [23], and the crystal lattice strains were determined through the Williamson–Hall method [24]. In order to determine the phases quantitatively, MAUD program [25] (based on the Rietveld method) was used. The calculated Rietveld reliability parameters were: $S$=2.2, $R_w$(%)=12.5, $R_{wnb}$(%)=12.3, $R_b$(%)=9.5, $R_{exp}$(%)=5.7 for XRD corresponding to as made sample, and $S$=2.1, $R_w$(%)=16.3, $R_{wnb}$(%)=15.7, $R_b$(%)=13.9, $R_{exp}$(%)=7.7 for XRD of the sample after the phase transformation.

MS at room temperature was applied under transmission geometry with a standard constant acceleration spectrometer using a 10 mCi $^{57}$CoRh radioactive source. The isomer shifts were referred to α-Fe.

The measurement of mass magnetization as a function of applied magnetic field ($\sigma$ vs. $H$) at 300 K, and mass magnetization as a function of temperature ($\sigma$ vs. $T$) under ~7958 A/m applied magnetic field were performed using a commercial vibrating sample magnetometer.

The thermal analysis was carried out in a differential scanning calorimeter under dynamic Ar atmosphere. The heating was performed at 5 °C/min scan rate. The powder sample was placed in a closed aluminum paper and sealed in aluminum pan.

In situ X-ray absorption near edge structure (XANES) spectra at Fe K-edge were collected in transmission mode using the D06A-DXAS beamline at Laboratorio Nacional de Luz Síncrotron (LNLS), Campinas, Brazil. During the experiment the sample was placed in an oven applying 5 °C/min heating rate. The XANES data analysis was performed using *Athena* software by subtracting a linear background and rescaling the absorbance by normalizing the difference between the baseline and the post-edge absorption. The calibration of the energy scale was performed by measuring metallic foil of Fe. The sample for XANES experiments was prepared in the form of 5 mm-diameter pellet using standard pressure procedure. Boron nitride powder was mixed with previously sieved 10 μ-mesh powder of the sample under research. The mass of the powder was estimated to optimize the absorption jump.

## 3. Results and discussion

Fig. 1 shows the XRD patterns of powders corresponding to the sample before and after being submitted to the heating. As it can be seen from the XRD pattern of the sample before heating (as made sample), the crystalline planes corresponding to a hexagonal ferrite $SrFe_{12}O_{19}$ (S.G. $P_{63/mmc}$, sys. hexagonal, $a$=0.588 nm, $c$=2.304 nm [26]) as main phase, and $SrCO_3$ (S.G. R-3m, sys. rhombohedral, $a$=0.5092 nm, $c$=0.9530 nm [27]) and maghemite ($\gamma$-$Fe_2O_3$) (S.G. Fd-3m, sys. cubic, $a$=0.835 nm [28]) as secondary phases were identified (Fig. 1a). After heating up to 625 °C the phase transformation was corroborated. The peaks corresponding to the magnetite ($Fe_3O_4$) as main phase (S.G. Fd-3m, sys. cubic, $a$=0.8394 nm [29]) and $SrCO_3$ as secondary phase were found (Fig. 1b).

It is possible to emphasize that the composition of the as made sample determined by XRD (Fig. 1a) is closely related to the synthesis procedure used. Even though the thermal treatment under oxygen flow allows decreasing the temperature needed to obtain hexagonal ferrite $SrFe_{12}O_{19}$, the as made sample is a mix of phases. About 40% of the sample is formed by $\gamma$-$Fe_2O_3$ and $SrCO_3$. Both are the inorganic precursors of the hexagonal ferrite. Similar effects were observed when the method of synthesis was the traditional sol–gel (thermal treatment in air atmosphere) [30].

Following the traditional steps of the sol–gel method, a thermal treatment with temperatures between 1050–1100 °C is necessary to complete the transformation of the inorganic phase precursors ($\gamma$-$Fe_2O_3$ and $SrCO_3$) to hexagonal ferrite [14]. The more accurate reports indicate that the hexagonal ferrite begins to form between 550 °C and 600 °C [14,31] and the process is maximum over 780 °C [22]. When the traditional thermal treatment is used (in air atmosphere) the temperature necessary to obtain $SrFe_{12}O_{19}$ is high. This happens because the decomposition of the organic material leads to emission of $CO_2$ gas which recombines with $Sr^{2+}$ to form

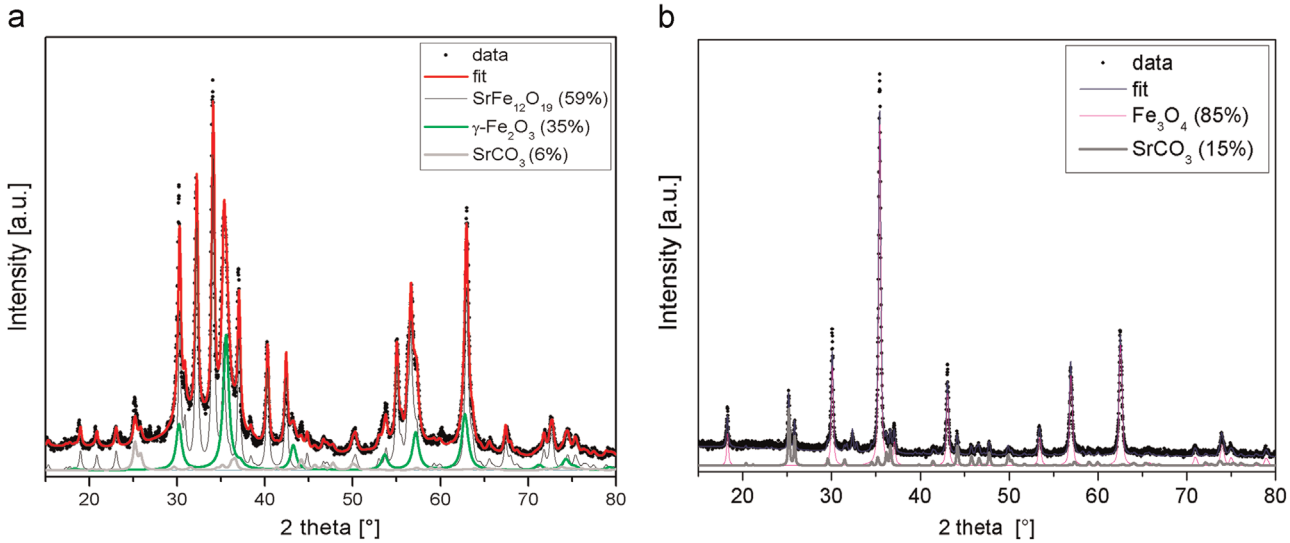


**Fig. 1.** XRD patterns: (a) as made sample before and (b) after its heating up to 625 °C.

$SrCO_3$. Then a temperature near 700 °C is needed to decompose the carbonate. In this situation, the $Sr^{2+}$ ion is capable to diffuse to form the hexagonal ferrite. Nevertheless, the use of oxygen flow during the thermal treatment diminishes the possibility of the $SrCO_3$ formation. The $CO_2$ gas resulting from the decomposition of the organic material is continuously evacuated with an $O_2$ flow. In this manner, the anchor of the $Sr^{2+}$ ion in the form of carbonate is avoided. This latter fact as well as a highly oxidizing atmosphere favors the ion reactivity to form $SrFe_{12}O_{19}$.

When the as made sample was heated up to 625 °C under confinement conditions (in an enclosed capsule) the phase transformation with the corresponding change of the oxidation state of the iron ions was verified. As it can be seen from Fig. 1, the $SrFe_{12}O_{19}$ and γ-$Fe_2O_3$ phases (~59% and ~35% of the sample, respectively) were transformed into $Fe_3O_4$ and $SrCO_3$ phases (~85% and ~15% of the sample, respectively). In addition, the amount of amorphous material also changed. For the as made sample the amorphous component was ~37% of the total area under the curve of the XRD pattern, while it was not detected when the phase transformation took place.

It is well known that the thermal decomposition of the amorphous organic material plays an important role in the mechanism of phase transformation. In this sense, the reduction from $Fe^{3+}$ to $Fe^{2+}$ is a consequence of how the heating up to 625 °C was carried out. In particular, the as made sample was confined in a capsule of aluminum and the gases of decomposition of the $SrFe_{12}O_{19}$ organic precursor saturated the atmosphere in which the sample was heated. It is necessary to emphasize that the organic component prevails in the sample composition because the temperature of synthesis (250 °C) is not enough to decompose it. Further, when the sample was subjected to heating (up to 625 °C) the amorphous organic material was decomposed forming carbon monoxide ($CO^-$) and nitrogen monoxide ($NO^-$). $CO^-$ and $NO^-$ are free radicals with one unpaired valence electron. The atmosphere became rich in these two anions (source of electrons), which induced the reduction of $Fe^{3+}$ to $Fe^{2+}$. A similar mechanism (reduction of $Fe^{3+}$ by $CO^-$) has been verified in the phase transformation of maghemite [32] and hematite [33,34].

Fig. 2 shows the calorimetric evolution of the as made sample under a continuous heating regime from 50 to 625 °C. The calorimetric curve reveals exothermic transformations occurring just after 550 °C, which could be attributed to the phase transition occurred.

In addition, σ vs. $H$ and σ vs. $T$ curves of the as made sample and after phase transformation are shown in Fig. 3. From σ vs. $T$ curves

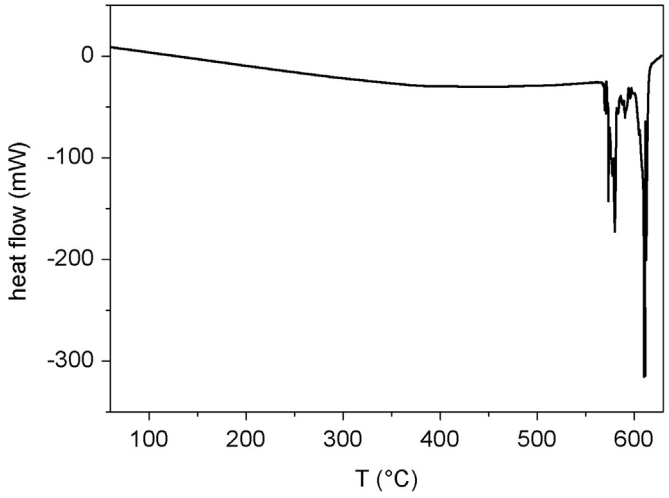


**Fig. 2.** DSC curve of as made sample.

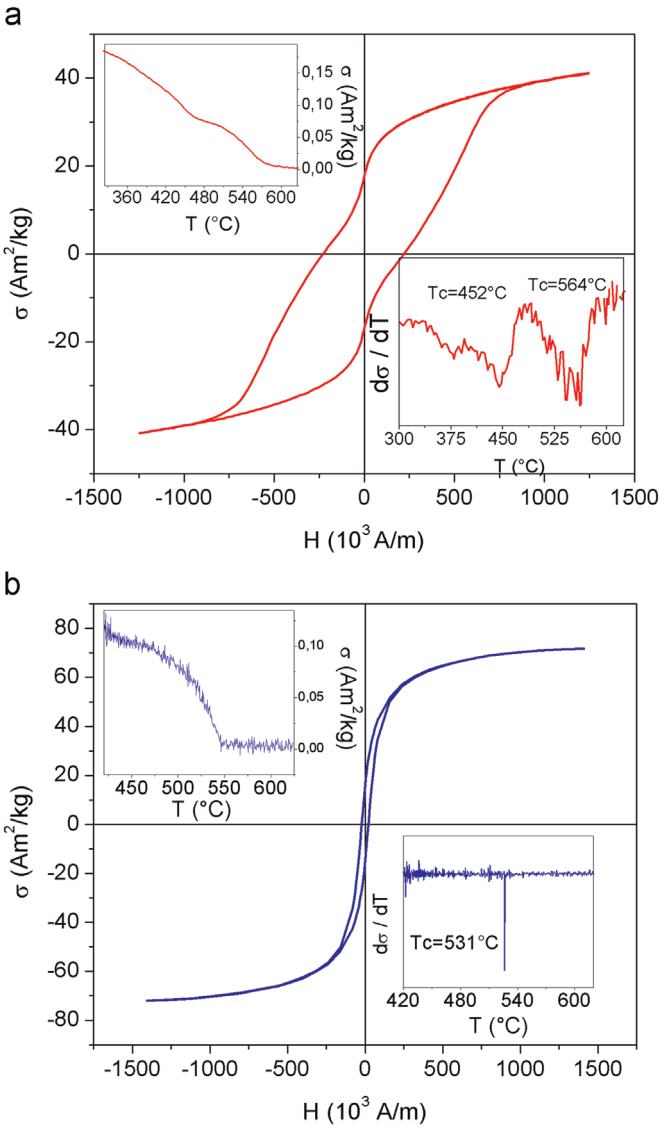


**Fig. 3.** σ vs. $H$ curve corresponding to the sample before (a) and after (b) phase transformation. σ vs. $T$ curve (upper inset), and the first derivative curve (bottom inset) corresponding to both samples are shown ($T_C$ of magnetic phases are indicated).

the Curie temperatures ($T_C$) can be determined and, therefore, the magnetic phases can be identified. From the first derivative of σ vs. $T$ curve of the as made sample (the bottom inset of Fig. 3a) two transition temperatures, 452 °C and 564 °C, were determined. The value of 452 °C is similar to the $T_C$ reported for the $SrFe_{12}O_{19}$ phase [1,2,35], while the value of 564 °C is close to the $T_C$ reported for γ-$Fe_2O_3$ [28]. The upper inset of Fig. 3b shows the $M$ vs. $T$ curve corresponding to the sample after phase transformation. It was noticed that this curve exhibited different behavior in comparison with the one of the as made sample where the only magnetic transition appeared at 531 °C. This temperature is associated with the $T_C$ of $Fe_3O_4$ [36].

On the other hand, the contribution of the $SrFe_{12}O_{19}$ (magnetically hard) [1] and γ-$Fe_2O_3$ (magnetically soft) [28] defined the shape of the σ vs. $H$ curve corresponding to as made sample (Fig. 3a). The measured value of coercivity, $H_c$=223 kA/m, is lower than the reported for $SrFe_{12}O_{19}$ (~360 kA/m, [35,37]) and higher than the reported for γ-$Fe_2O_3$ (near 350 Oe [38]). Meanwhile the specific magnetization ($\sigma_S$) determined for the as made sample is close to the one reported for samples containing similar

composition (~60% $SrFe_{12}O_{19}$ and ~40% γ-$Fe_2O_3$) [37].

We observed that the $\sigma$ vs. $H$ curve corresponding to the sample after the phase transformation (Fig. 3b) showed an increase of $\sigma_S$ and a reduction of $H_c$. It is a typical hysteresis loop of a magnetically soft material ($H_c$=12.8 kA/m). The value of $H_c$ is similar to the reported value for $Fe_3O_4$ phase [39]. The observed value of $\sigma_S$, 72 $Am^2/kg$, is close to the reported for this phase [38,40].

We suggest that $SrFe_{12}O_{19}$ transformation to $Fe_3O_4$ and $SrCO_3$ occurred by a combination of, at least, three factors such as: (i) the presence of stress in the crystal lattice of $SrFe_{12}O_{19}$ due to low synthesis temperature, (ii) the reduction of $Fe^{3+}$ to $Fe^{2+}$ during the heating up to 625 °C, and (iii) the similarity of the coordination spheres of the iron atoms present in the S-block of $SrFe_{12}O_{19}$ and $Fe_3O_4$ (both structures are of spinel type). These factors are discussed below.

The analysis of the XRD pattern associated with $SrFe_{12}O_{19}$ hexagonal ferrite of the as made sample allowed determining the average crystallite size of this phase. The calculated size was around 8 nm wide and about 13 nm length. The dimensions of these crystallites are different from the platelets of hexagonal ferrites (which have a much greater length than width [14,41,42]) obtained by traditional methods. The energy involved in low temperature synthesis of the as made sample was just enough for a nucleation and partial growth of the phase.

The (220) and (205) reflections were selected to determine the size of the nanoparticles in the directions of the $c$ and $a$ crystallographic axes of the hexagonal symmetry, respectively. For each of these crystal planes, the Scherrer equation [23] was applied with a deconvolution of the diffraction peaks from a silicon standard NBS 640 (certificated pattern) to subtract the instrumental effects.

The term $L_{hkl}$ present in the Scherrer equation should be interpreted as an average of the dimensions (of the crystal) perpendicular to the diffraction plane. The (220) plane is parallel to the $c$ axis of $SrFe_{12}O_{19}$ crystal and $L_{220}$ provides information on the length of the hexagonal ferrite particle. Meanwhile, the value of $L_{205}$ expresses approximately its width.

The size of $SrFe_{12}O_{19}$ nanoparticles forming the as made sample is about 10–15 times smaller than the hexagonal ferrite particles obtained by traditional chemical and sol–gel methods [14, 31, 43]. The shape (width/length ratio) and the size of $SrFe_{12}O_{19}$ nanoparticles of the studied sample can be an indication of the existence of disorder and strains in the crystal lattice of this phase. The analysis using Williamson–Hall (W–H) graph of XRD patterns before and after the phase transformation provides qualitative and semiquantitative information on this aspect [24].

Fig. 4 shows the W–H graphs corresponding to the main phase of the XRD patterns of the as made sample and after its phase transformation. These graphs, $\beta \cdot \cos\theta$ vs. $\sin\theta$, were obtained from the information provided by the reflections corresponding to these crystalline phases ($SrFe_{12}O_{19}$ and $Fe_3O_4$), where $\beta$ is the full width at half maximum of the peaks, and $\theta$ is the reflection of Bragg positions. From the slope of the line ($S$), microdeformations (MD) of crystal can be calculated by using the following relationship among these parameters: MD = $S/4$ [24].

The linear fit to the W–H graph corresponding to the $SrFe_{12}O_{19}$ phase showed a marked slope associated with the MD present in the crystal of the strontium hexaferrite. The calculated value of the MD, $2.6 \cdot 10^{-1}$, is two orders of magnitude difference respect to the value corresponding to metallic oxides without strain in the lattice [44]. It is worth highlighting that these deformations are not an effect of size of nanoparticle, because if so one would get a line without slope [24]. The strain in the lattice of $SrFe_{12}O_{19}$ can be associated with an incomplete formation of the interstitial sites occupied by metallic ions (for example, the $Fe^{3+}$ bipyramidal site of the rhombohedral block) [1]. The incomplete formation can be due to an insufficient energy for the diffusion of the ions into the oxygen packing because of the low temperature of the synthesis of the sample (250 °C).

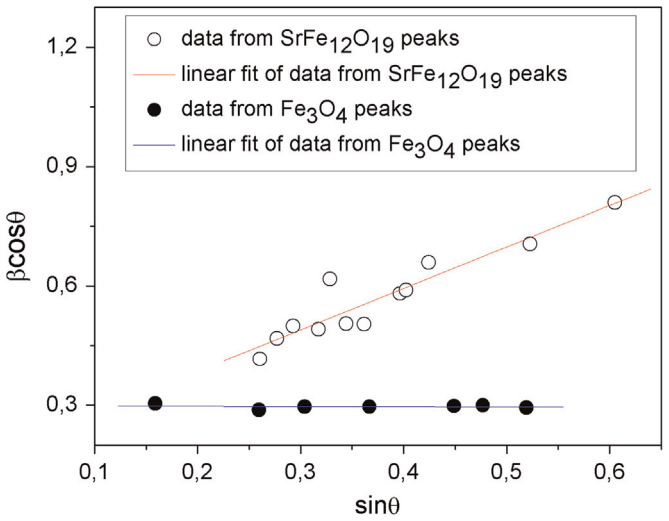


**Fig. 4.** Williamson–Hall graphs obtained from the X-ray reflections of $SrFe_{12}O_{19}$ (the main phase before the structural change) and $Fe_3O_4$ (the main phase after the structural change).

Meanwhile the linear fit to the W–H graph corresponding to the main phase of the sample after the structural change ($Fe_3O_4$ phase) showed a straight line almost without slope (Fig. 4). The slope close to zero indicates the absence of microdeformations and strains in the crystal lattice of $Fe_3O_4$ phase. This fact is an evidence of that a more stable material was obtained after the phase transformation. The change of the slopes also indicates that the phase transformation minimized the energy of the system. We suggest that the phase transformation occurred by means of a diffusion process in solid state. It was possible due to the similarity among the compact packing of oxygen ions which form the main phases of the initial and final products.

The $SrFe_{12}O_{19}$ ferrite (Fig. 5) is a packing of oxygen ions formed by two kinds of blocks with different symmetry containing the metals [1,2]. The block containing the $Sr^{2+}$ ion is a hexagonal packing (R-block) in which three types of interstitial sites (octahedral, tetrahedral and bipyramidal) are occupied by $Fe^{3+}$ ions. The other block has a cubic symmetry of spinel type (S-block). The latter is formed by the same type of compact cubic packing that forms $Fe_3O_4$ phase. Both the S-block of the hexaferrite and the structure of $Fe_3O_4$, contain octahedral and tetrahedral sites occupied by iron ions. Taking into account the microdeformations and strains detected in the crystal lattice of the $SrFe_{12}O_{19}$ phase, it is possible that the heating up to 625 °C of the as made sample induces a diffusion of the iron ions from interstitial sites of lower symmetry, such as the bipyramidal sites present in the R-block, to the sites with higher symmetry (octahedral and tetrahedral). Such diffusion could deform the R-block until its disappearance, letting the $Sr^{2+}$ ion freely move to form other environment, while iron ions would be contained in the cubic packing defined by octahedral and tetrahedral interstitials sites. On the other hand, it is worth highlighting that the experimental results proved that a reduction from $Fe^{3+}$ to $Fe^{2+}$ during the heating occurred as well. The change of the oxidation state of the iron ion caused a change of its ionic radius which favors the diffusion process and the crystalline rearrangement explained before (the change from hexagonal to cubic symmetry).

The analysis of Mössbauer spectra (MS) provided clear evidence of the phase transformation as well as the reduction of $Fe^{3+}$

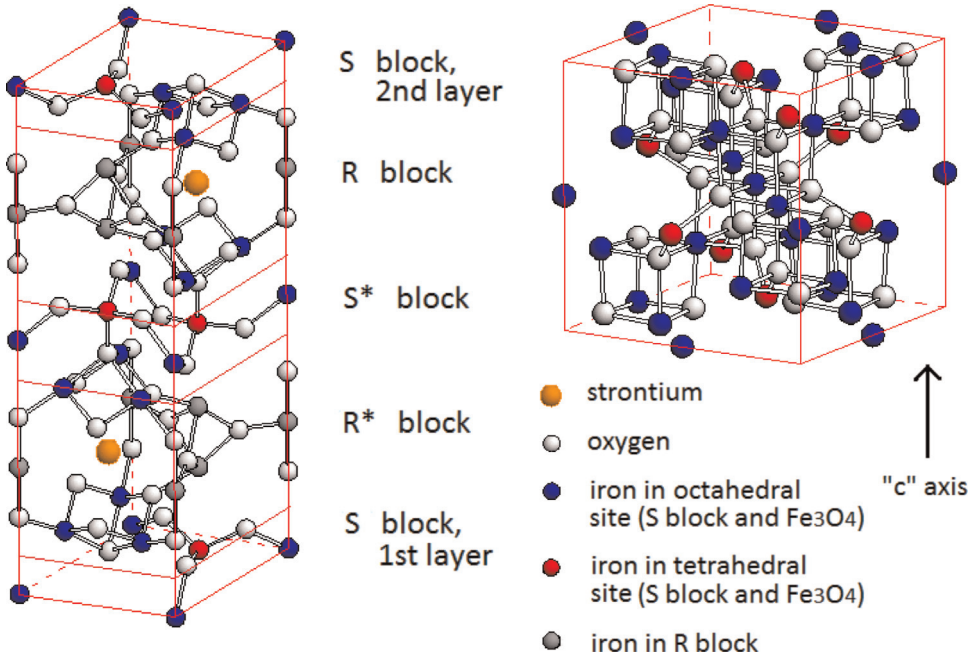


**Fig. 5.** Unit cells of $SrFe_{12}O_{19}$ (left) and $Fe_3O_4$ (right). The crystal structure of $SrFe_{12}O_{19}$ could be represented as a sequence of S- and R-blocks (S R S* R*). The asterisk indicates a 180° rotated block [1]. The S-block of $SrFe_{12}O_{19}$ and the unit cell of $Fe_3O_4$ have a similar spinel structure.

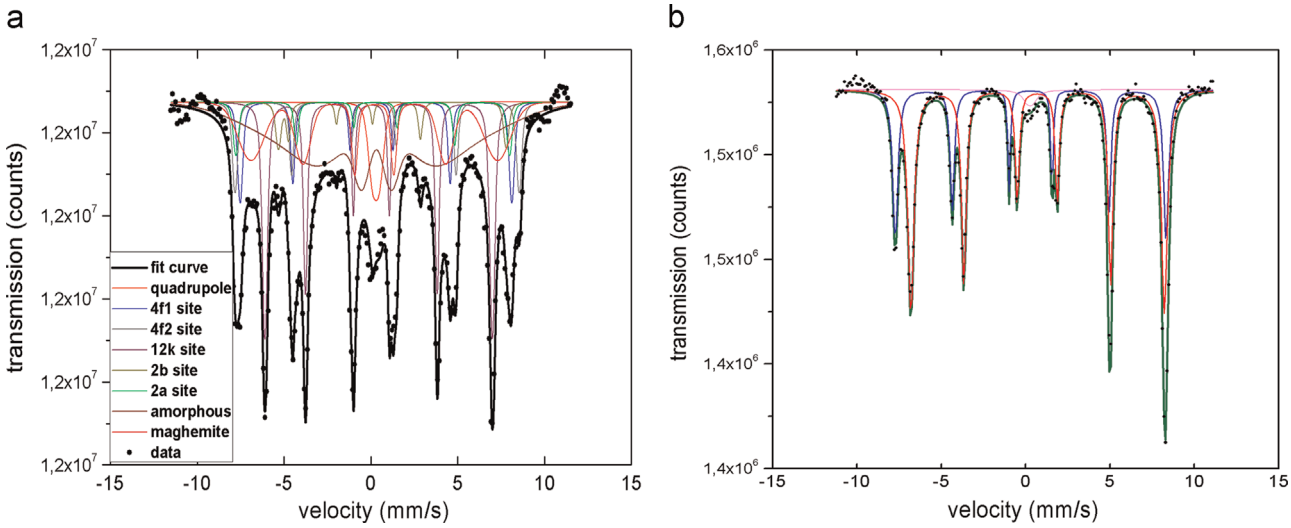


**Fig. 6.** Mössbauer spectra corresponding to the sample before (left) and after (right) the phase transformation.

**Table 1**
Mössbauer parameters corresponding to the fit of the as made sample. Errors in the isomer shift ($\delta$), quadrupole splitting ($\Delta$) are close to 0.01 mm/s. Errors in the hyperfine field ($B_{hf}$) and the fraction area ($A$) do not exceed 5%.

| Identification | δ (mm/s) | Δ (mm/s) | $B_{hf}$ (T) | A (%) |
|---|---|---|---|---|
| $SrFeO_{19}$ | | | | |
| 12k site | 0.34 | 0.42 | 40.7 | 19.5 |
| $4f_1$ site | 0.27 | 0.26 | 50.7 | 8.6 |
| $4f_2$ site | 0.37 | 0.1 | 53.1 | 7.6 |
| 2a site | 0.2 | −0.16 | 50.8 | 4.5 |
| 2b site | 0.25 | 2.18 | 42.3 | 3.4 |
| Amorphous | 0.42 | 0 | 32.4 | 35.4 |
| $\gamma$-$Fe_2O_3$ | 0.30 | 0 | 43.9 | 16.4 |
| Quadrupole interaction | 0.30 | 0.46 | – | 4.4 |

to $Fe^{2+}$. The fitting procedure (Fig. 6) of the spectrum of the as made sample was developed in accordance with the model proposed previously by us [21]. As it can be seen from Table 1, only isomer shifts corresponding to $Fe^{3+}$ were detected (~0.3 to 0.4 mm/s). The complex spectrum was resolved as it follows. $Sr_{12}Fe_{12}O_{19}$ phase was successfully fitted by five iron components (sextets) corresponding to five crystallographic sites: 12k, $4f_1$, $4f_2$, 2a and 2b. Additionally, a distributed sextet corresponding to $Fe^{3+}$ in maghemite and a highly distributed sextet attributed to amorphous part of the sample were introduced during the fitting procedure as well as a doublet. The latter component could be due to iron in paramagnetic(superparamagnetic) phase of small amount. Sextets represent magnetic (dipolar) interactions, meanwhile doublet is a quadrupolar interaction.

The fit to the MS corresponding to the sample after the phase transformation is shown in Fig. 6, the fitted parameters are summarized in Table 2. Values of isomer shifts equal to 0.3 mm/s and 0.7 mm/s were determined. The lower value is characteristic of $Fe^{3+}$ species in tetrahedral environment (site A, blue), meanwhile the higher value is a mix contribution of $Fe^{3+}$ and $Fe^{2+}$ ions coexisting in octahedral environment (site B, red) of $Fe_3O_4$ [45].

**Table 2**
Mössbauer fitted parameters corresponding to the sample after the phase transformation.

| Identification | δ (mm/s) | Δ (mm/s) | $B_{hf}$ (T) | A (%) |
|---|---|---|---|---|
| $Fe_3O_4$ | | | | |
| Site A | 0.28 | −0.05 | 49.9 | 37.3 |
| Site B | 0.70 | 0.05 | 46.9 | 59.9 |
| Quadrupole interaction | 0.3 | 0.4 | – | 3 |

Additionally, the determined values of hyperfine magnetic field and quadrupole splitting are characteristic of the magnetite. Both quadrupole interactions (Tables 1 and 2) with similar hyperfine parameters probably correspond to the nonmagnetic $SrFeO_{2.74}$ [20] whose small amount was hardly observed by XRD.

After the effective determination of A and B occupied sites (the relative areas) by iron populations, it is possible to estimate if the crystal structure of the iron oxide presents vacancies [46]. The calculated ratio is $r$=A:B=0.62 and, using the formula reported by Voogt et al. ($\delta=[2r-1]/[6r+5]$) [46], we estimated how much the magnetite's stoichiometry deviates from its theoretical value. The obtained formula was $Fe_{2.97}O_4$, almost the theoretical one, is consistent with the information obtained from the W–H graph indicating an absence of strains in the crystal lattice (a straight line, Fig. 4).

The phase transformation was also registered in the measurements at Fe K-edge using DXAS technique. In Fig. 7a some XANES curves (of the as made sample) acquired during DXAS measurements are shown. As it can be seen, when the temperature increased the position of the absorption edge of the spectra was shifted to lower energies. This fact is a direct indication of a change of oxidation state of the sample since XANES signal is highly sensitive to such a change. Moreover, starting the experiment with the sample having only $Fe^{3+}$ ions, a shift of absorption edge that indicates an iron reduction process [47] during the heating procedure was observed. As it can be appreciated from Fig. 7b, the absorption edge of the as made sample was in agreement with that of $SrFe_{12}O_{19}$ where only $Fe^{3+}$ ions are present. It is an indication that in the sample the iron species were in the same oxidation state (3+). For comparison purpose, we also measured the XANES signal of FeO ($Fe^{2+}$ ions only) and magnetite ($Fe_3O_4$ where $Fe^{3+}$ and $Fe^{2+}$ ions coexist). It was observed that the reference sample with $Fe^{2+}$only had its absorption edge shifted to the left, meanwhile magnetite had its absorption edge between FeO and $SrFe_{12}O_{19}$ (Fig. 7b) as expected.

In addition, we performed linear combination analysis of the XANES spectra to evaluate the amount of magnetite formed. For this purpose we adapted a simple approximation model taking into account two standards: the XANES signals of $SrFe_{12}O_{19}$ and $Fe_3O_4$. The energy interval of the observed curve used to perform the linear combination was between −30 eV and 200 eV around absorption edge. In Fig. 7c, we show $Fe_3O_4$ amount in the course of the reduction process. Even though these values are not quantitatively exact (note our approximation model), this plot gives us qualitatively valuable information because it reveals the dynamics of magnetite formation as a function of temperature. It can be seen that a significant increasing of the amount of the magnetite occurred at nearly 200 °C, upon approximately 450 °C the amount was almost unchangeable, after that it grew up to 570 °C. In other words, two temperature regions where the magnetite amount changed noticeably were observed.

The first increase of the amount of $Fe_3O_4$ at ~200 °C (Fig. 7c) was due to the beginning of the process of the reduction of $Fe^{3+}$ in the S- and R-blocks of $SrFe_{12}O_{19}$. The reduction of $Fe^{3+}$ to $Fe^{2+}$ led

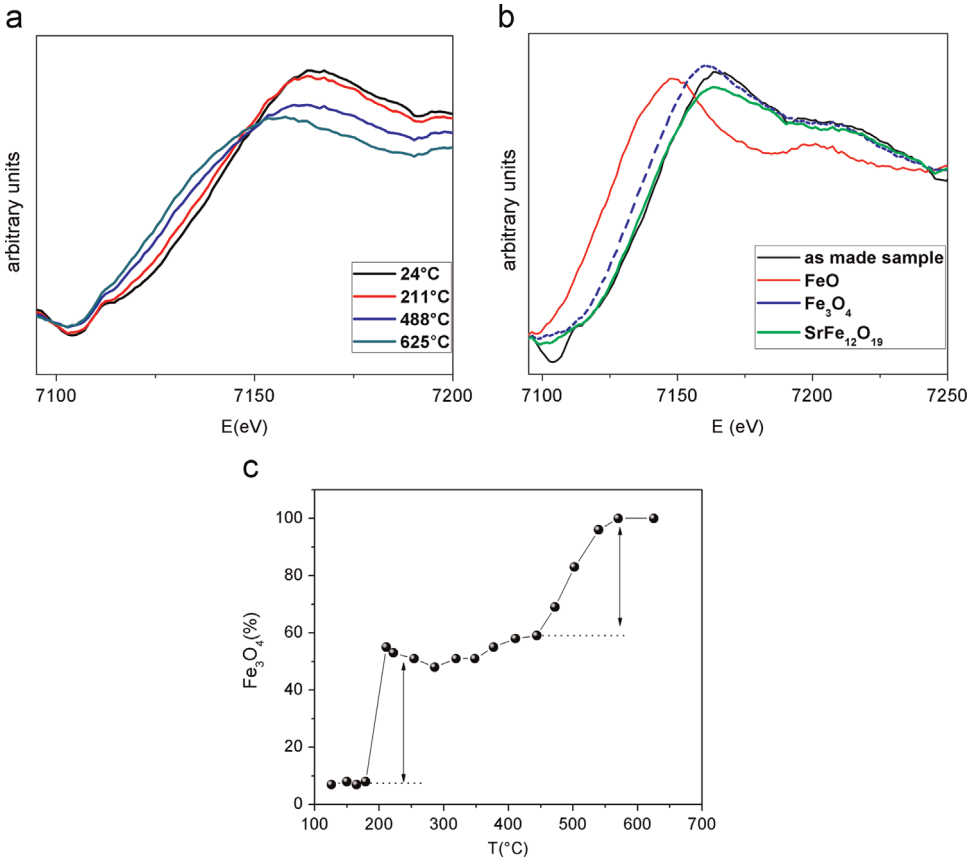


**Fig. 7.** DXAS measurements: (a) Fe K-edge XANES signal acquired at different temperatures for the as made sample; (b) XANES signals of as made sample and the references (FeO, $Fe_3O_4$, $SrFe_{12}O_{19}$) at room temperature; (c) amount of $Fe_3O_4$ extracted from the linear combination analysis of the XANES spectra during the heating.

to an increase of iron ion radius that induced the change of the symmetry of the crystal lattice. This process was corroborated by the existence of strains in the lattice of the hexagonal ferrite (Fig. 4). Among other causes, these strains were due to an unstable position of iron ions situated in bipyramidal site of R-blocks of $SrFe_{12}O_{19}$. When the sample was heated above its $T_C$, another jump took place (~450 to 570 °C, Fig. 7c). The thermal agitation of iron atoms from bypiramidal sites became important that facilitated the migration of these ions to octahedral and tetrahedral sites. The thermal agitation and the change of ionic radius of the iron were the factors that facilitated the diffusion of these ions into the ion packing of oxygen and induced the phase transformation.

## 4. Conclusions

When hexagonal ferrite $SrFe_{12}O_{19}$, obtained at low temperature (250 °C) under oxygen flux was heated up to 625 °C in confinement conditions, it was transformed in magnetite ($Fe_3O_4$) as main phase, and strontium carbonate ($SrCO_3$) as secondary phase. This phase transformation was verified using XRD, Mössbauer spectroscopy, DXAS and magnetic measurements. The XRD analysis confirmed the existence of the strain and microdeformations in the crystal of the $SrFe_{12}O_{19}$ and the absence of them in the material after the transformation. The Mössbauer spectroscopy and DXAS provided evidences of ion $Fe^{3+}$ reduction to $Fe^{2+}$ and confirmed the crystallographic phase identification of magnetite as product of the phase transformation. The transformation occurred by a combination of three factors: (i) the presence of stresses in the crystal lattice of $SrFe_{12}O_{19}$ due to low synthesis temperature, (ii) the reduction of the $Fe^{3+}$ to $Fe^{2+}$ during the heating up to 625 °C, and (iii) the similarity of the coordination spheres of the iron atoms present in the S-block of $SrFe_{12}O_{19}$ and $Fe_3O_4$ (both structures are of spinel type). Such factors complemented each other and determined the reported phase transformation.

## Acknowledgment

We acknowledge the financial support of CONICET, Argentina (PIP 11220120100462), as well as the financial assistance of LNLS, Campinas-SP, Brazil (LNLS Project DXAS11734).We appreciate the help of E.J. Lede in the DXAS measurements. We thank Dr. L.M. Socolovsky.

## References

[1] H. Kojima, Chapter 5: Fundamental properties of hexagonal ferrites with magnetoplumbite structure, in: E.P. Wohlfarth (Ed.), Ferromagnetic Materials, vol. 3, North-Holland Publishing Company, Amsterdam, 1982.
[2] J. Smit, H.P. Wijn, Ferrites: Physical Properties of Ferrimagnetic Oxides in Relation to Their Technical Applications, N.V. Philips' Gloeilampenfabrieken, Eindhoven, 1959.
[3] M. Matsuoka, M. Naoe, J. Appl. Phys. 57 (1985) 4040.
[4] R.H. Victora, J. Appl. Phys. 63 (1988) 3423.
[5] E. Lacroix, P. Gerard, G. Marest, M. Dupuy, J. Appl. Phys. 69 (1991) 4770.
[6] F. Walz, J. Rivas, D. Martinez, H. Kronmuller, Phys. Status Solid A 143 (1994) 137.
[7] T.G. Kuz'mitcheva, L.P. Ol'khovik, V.P. Shabatin, IEEE Trans. Magn. 31 (1995) 800.
[8] K. Haneda, H. Kojima, J. Am. Ceram. Soc. 57 (1974) 68.
[9] J.C. Bernier, Mater. Sci. Eng. A 109 (1989) 233.
[10] M. Matsumoto, A. Morisako, T. Haeiwa, K. Naruse, T. Karasawa, IEEE Trans. J. Magn. Jp. 6 (1991) 648.
[11] R. Martinez Garcia, E. Reguera Ruiz, E. Estevez Rams, R. Martinez Sanchez, J. Magn. Magn. Mater. 223 (2001) 133.
[12] E. Estevez Rams, R. Martinez Garcia, E. Reguera, H. Montiel Sanchez, H. Y. Madeira, J. Phys. D: Appl. Phys. 33 (2000) 2708.
[13] R. Martinez Garcia, E. Reguera Ruiz, E. Estevez Rams, Mater. Lett. 50 (2001) 183.
[14] W. Zhong, W. Ding, N. Zhang, J. Magn. Magn. Mater. 168 (1997) 196.
[15] M. Sivakumara, A. Gedankena, W. Zhongb, Y.W. Dub, D. Bhattacharyac, Y. Yeshurunc, I. Felner, J. Magn. Magn. Mater. 268 (2004) 95.
[16] S. Alamolhoda, S.A. Seyyed Ebrahimi, A. Badiei, J. Magn. Magn. Mater. 303 (2006) 69.
[17] D.D. Zaitsev, S.E. Kushnir, P.E. Kazin, Yu.D. Tretyakov, M. Jansen, J. Magn. Magn. Mater. 301 (2006) 489.
[18] M.M. Hessien, M.M. Rashad, K. El-Barawy, J. Magn. Magn. Mater. 320 (2008) 336.
[19] D. Primc, D. Makovec, D. Lisjak, M. Drofenik, Nanotechnology 20 (2009) 315605.
[20] K.A. Mangai, M. Priya, M. Rathnakumari, P. Sureshkumar, J. Appl. Spectrosc. 81 (3) (2014) 519–524.
[21] R. Martínez-García, V. Bilovol, L.M. Socolovsky, K. Pirota, J. Magn. Magn. Mater. 323 (2011) 3022.
[22] C. Surig, K.A. Hempel, D. Bonnenberg, IEEE Trans. Magn. 130 (1994) 4092.
[23] B.E. Warren, X-ray Diffraction, Dover Publications, inc., New York, 1990.
[24] G.K. Williamson, W.H. Hall, Acta Metall. 1 (1953) 22.
[25] < /http://www.ing.unitn.it/maud/ >.
[26] K. Kimura, M. Ohgaki, K. Tanaka, H. Morikawa, F. Marumo, J. Solid State Chem. 87 (1990) 186.
[27] K.O. Stromme, Acta Chem. Scand. A 29 (1975) 105.
[28] A.H. Morrish, Morphology and Physical Properties of Gamma Iron Oxide, University of Manitoba, Winnipeg, Canada, 1979.
[29] W.D. Derbyshire, H.J. Yearian, Phys. Rev. 112 (1958) 1603.
[30] E. Estévez Rams, R. Martínez-García, E. Reguera Ruíz, J. Phys. D: Appl. Phys. 33 (2000) 2708.
[31] A. Vijayalakshmi, N.S. Gajbhiye, J. Appl. Phys. 83 (1998) 400.
[32] Hoang Tri Hai, J. Colloid Interface Sci. 341 (2010) 194.
[33] L.S. Darken, P.W. Gurry, J.Am. Chem. Soc. 68 (1946)79 68 (1946).
[34] V. Osterhout, in: D.C. Craik (Ed.), Magnetic Oxides, Wiley, New York, 1975.
[35] M. Sivakumara, A. Gedankena, W. Zhongb, Y.W. Dub, D. Bhattacharyac, Y. Yeshurunc, I. Felnerd, J. Magn. Magn. Mater. 268 (2004) 95.
[36] A. Chakraborty, J. Magn. Magn. Mater. 204 (1999) 57.
[37] M.M. Hessien, M.M. Rashad, K. El-Barawy, J. Magn. Magn. Mater. 320 (2008) 336.
[38] Hoang Tri Hai, Hiroaki Kura, Migaku Takahashi, Tomoyuki Ogawa, J. Colloid Interface Sci. 341 (2010) 194.
[39] H. Iida, K. Takayanagi, T. Nakanishi, T. Osaka, J. Colloid Interface Sci. 314 (2007) 274.
[40] T.J. Daou, G. Pourroy, S. Begin-Colin, J.M. Greneche, C. Ulhaq-Bouillet, P. Legare, P. Bernhardt, C. Leuvrey, G. Rogez, Chem. Mater. 18 (2006) 4399.
[41] R. Martínez-García, E. Estevez Rams, E. Reguera Ruiz, R. Martínez Sánchez, Acta Microsc. 8 (2) (1999) 62.
[42] R. Martínez-García, E. Reguera Ruíz, E. Estévez Rams, R. Martínez Sánchez, J. Magn. Magn. Mater. 223 (2001) 133.
[43] C. Sürig, K.A. Hempel, D. Bonnenberg, Appl. Phys. Lett. 63 (1992) 2836.
[44] D.G. Lamas, G.E. Lascalea, R.E. Juárez, M.F. Bianchetti, M.E. Fernández de Rapp, N.E. WalsÖe de Reca, Matéria 8 (2003) 213.
[45] E. Murand, J.H. Johnston, Mossbauer Spectroscopy Applied to Inorganic Chemistry, in: G.J. Long (Ed.), Plenum Publishing Corporation, New York, 1987.
[46] F.C. Voogt, T. Fuji, P.J.M. Smulders, L. Nielsen, M.A. James, T. Hibma, Phys. Rev. B 60 (1999) 11193.
[47] D. Carta, M.F. Casula, A. Falqui, D. Loche, G. Mountjoy, C. Sangregorio, A. Corrias, J. Phys. Chem. C 113 (2009) 8606.